Calibration of Laser Range Finders for Mobile Robot Localization in ITER

Tiago Sousa[1], Alberto Vale[2] and Rodrigo Ventura[3]
[1]*Instituto Superior Técnico, Universidade de Lisboa, Av. Rovisco Pais 1, 1049-001, Lisboa, Portugal*
[2]*Instituto de Plasmas e Fusão Nuclear, Instituto Superior Técnico, Universidade de Lisboa, Av. Rovisco Pais 1, 1049-001, Lisboa, Portugal*
[3]*Laboratório de Robótica e Sistemas em Engenharia e Ciência, Instituto Superior Técnico, Universidade de Lisboa, Av. Rovisco Pais 1, 1049-001, Lisboa, Portugal*

Keywords: Laser Range Finder, Calibration, Localization, ICP.

Abstract: Remote maintenance operations in the experimental fusion reactor ITER may require vehicle localization, for which one of the proposed methods is based on a network of Laser Range Finder sensor measurements. This localization method requires an accurate knowledge of each sensor pose (position and orientation). A deviation in sensor pose can compromise localization accuracy thereby recalibration procedure for the sensor poses is often necessary. This paper studies several calibration algorithms based on ICP. Simulation and experimental tests were carried out for different maps and situations regarding sensor pose uncertainty. The conclusion proposes the best suited algorithms for each scenario.

1 INTRODUCTION

Producing enough energy to cover our civilizational primary energy needs and living standards, has always been one of the main goals and focuses of our modern civilization. The current growth in energy supply demand has raised the concern on the environmental impact of current ways of energy production and lead to the discussion of reliable and new alternatives. Fusion power promises itself as a clean, and sustainable source of usable energy. The biggest challenge now is to prove that a large scale functionality and production is possible. The International Thermonuclear Experimental Reactor (ITER) is a multinational in-progress experimental project located in Cadarache, south of France and represents the next step of demonstration. Workers are not allowed to enter the ITER facilities during its operation and transportation of activated components (see Figure 1).

Instead, the nominal and maintenance operations (A. Tesini, 2008) will be handled completely remotely. Some of the critical operations include the transportation of shielded casks, that enclosures the load and spare parts by the Cask and Plug Remote Handling System (CPRHS) vehicles and Cask Transport System (CTS) (Darren Locke, 2014) vehicles and the operation of rescue vehicles such as the proposed Multi Purpose Rescue Vehicle (MPRV) (J. Soares, 2014) for inspection, repair and component replacement. To perform the previous and other tasks with minimal error margin, an accurate navigation method is needed due to the tight safety margins inside the building. The navigation uses the vehicles localization estimation (J. Ferreira, 2013) to autonomously maneuver the vehicle trough its path or to help a human operating it remotely. A network of Laser Range Finder (LRF) sensors are proposed, due to their immunity to magnetic fields that proliferate in near the Tokamak and high accuracy distance measurements

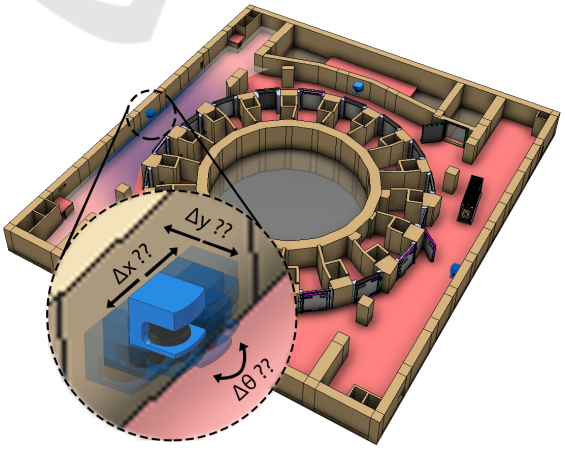

Figure 1: Problem illustration in ITER building.

Sousa T., Vale A. and Ventura R..
Calibration of Laser Range Finders for Mobile Robot Localization in ITER.
DOI: 10.5220/0005536505410549
In *Proceedings of the 12th International Conference on Informatics in Control, Automation and Robotics* (ICINCO-2015), pages 541-549
ISBN: 978-989-758-122-9

in long and short distances, which the localization estimation method is based and heavily reliant on.

Calibration is a problem that relies on most of the sensors, in particular, the ones used in high demanding accuracy applications. After the first calibration, every sensor might need a recalibration depending on some working condition factors such as level of tear, stability and wear suffering during operational time. Besides the general problems in calibration regarding sensor's own measurements, here the focus is on calibrating the measurements between a network of LRF sensors in such a way the measurements from different sensors could have a valid correspondence between them (see Figure 1). The devices are attached to environment walls to reduce the chance of electronics being damage by the radiation. A deviation of 100 mm in sensor position and 5° in orientation could cause as much as a deviation of about 120 mm (as stated in (J. Ferreira, 2013)) and 873 mm respectively in vehicle location. These deviations compromise maneuvers of hazard material transportation vehicles on narrow and tight spaces.

LRF sensors have becoming of widespread use in mobile robot systems because of its high accuracy distance measurements. Among LRF, other sensors such as cameras (IR and RGB) and odometry information are often used simultaneously to guide autonomous vehicles. Some methods for calibration between a camera and LRF have been proposed (Vincenzo Caglioti, 2008), other methods such as SLAM (Sebastian Thrun, 2008) use the odometry information along LRF readings in its localization algorithm. In the previous approach, after calibration, the results are given in the robots frame which is not static, so the readings might change with time. In ITER sensors are fixed to environment walls. When calibration procedure takes place, it is assumed that all measurements are derived from the map so no fix or moving outliers presence were considered. The only changes in LRF consecutive measurements should be associated with the sensor precision limits.

Some LRF calibration techniques have been proposed such as (Antone and Friedman, 2007), (K. Schenk, 2012) but all of them have one thing in common: they require physical access to the environment where the calibration takes place. Since no hand calibration is possible, the calibration procedure, like many other operations in ITER context, must be made entirely remotely. The Calibration techniques stated before, use static or moving objects (or humans) that must be asymmetrical to uniquely identify the target. That is not the case as the CTS vehicle features a symmetrical rectangular shape and uses a rhombic-like kinematics configuration for high maneuvering and flexibility making heading extraction not trivial.

Given the physical access constraints of ITER, a map description of the environment shall provide the valuable opportunity to check and compare where the LRF measurement data best fits on the map. Therefore the map layout description should be as accurate as possible to mitigate the impact of erroneous walls dimensions or unmapped areas/objects on results.

This paper is divided as follows: Section 2 presents the proposed solution. The implemented simulation environment is described in Section 4, preceded by the obtained results in Section 5. Finally, the last section is reserved for the conclusions discussion.

2 PROBLEM STATEMENT

In ITER, the optimal locations where the LRF sensors should be installed are determined beforehand by an algorithm in (J. Ferreira, 2013). As a consequence of sensor misplacement, measurements from distinct LRF lose correspondence between them. Address and solving this problem is the main focus and objective of the present work. This issue, where the exact position and orientation of the sensors are spoiled, can be caused by human error on installation procedure, erroneous map measurements or any other factor such as the ones mentioned in Section 1.

The pose P, for a given sensor in the network, includes its position coordinates (x_p, y_p) in meters and its orientation θ_p in angle degrees. Both are given in the map coordinate frame (x_w, y_w) as illustrated in Figure 2. Also a horizontal orientation is assumed (pitch and tilt not influential).

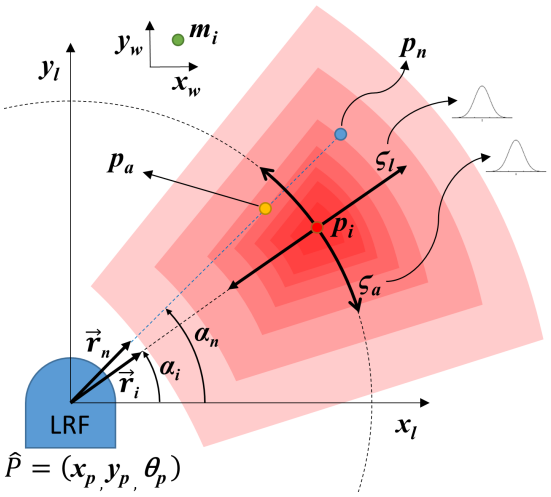

Figure 2: Variables involved in the problem description.

The LRF sensors return data in two dimensional polar coordinate system where the distance measurements $\|r_n\|$ and the associated angle α_i are given in device frame (x_l, y_l). Since the distance measurements are affected by noise, LRF returns $\|r_n\|$ measurements instead of the true $\|r_i\|$ yielding the p_n points. The objective is to estimate the absolute final pose, $\hat{P}_f$, of each sensor in the network that minimizes the mean quadratic error, e_{pp}, function in (1). The residual is composed by the point to point Euclidean distance between the transformed LRF measurements $T(\hat{P}_f, p_n)$ and the respective map closest points m_n. This is a difficult optimization problem due to several local minima existence.

$$e_{pp} = \underset{\hat{P}_f}{\operatorname{argmin}} \frac{1}{N} \sum_{n}^{N} \|T(\hat{P}_f, p_n) - m_n\|^2 \qquad (1)$$

3 PROPOSED SOLUTION

The proposed solution is a main algorithm that receives as input a map description, LRF measurement data, and an optional initial pose estimate $\hat{P}_i$. The uncertainty degree associated with this parameter leads to four different scenarios (denoted A, B, C, and D below) that specify the way the algorithm behave. In case an initial pose estimate is given (scenario A), the algorithm behaves locally trying to extract the best pose for the given measurements. Instead, if an initial pose estimate is not given at all (scenario D), the algorithm behaves globally on the map, assuming any pose is plausible. Other two intermediate scenarios (B, C) may occur whenever one parameter of the initial pose is missing.

3.1 Data Pre-processing

This first phase in the algorithm execution is common in every case scenario. By averaging raw data from multiple scans, it is possible to mitigate the errors in readings derived from the random errors in LRF devices. This way precision improves proportionally to the square root of the number of complete scans as stated in (Markus-Christian Amann, 2000). But before averaging, a normality test takes place to verify if data its well a modeled normal distributed population so an averaging metric could be meaningful in this context. The averaging method implemented uses a significant number of scans (at least one hundred) to determine the average value μ, and the standard deviation σ. Using a window interval, w, given by (2) it was possible to reject the extreme values before applying the average metric. As average metric is strongly influenced by extreme values, and after some experimentation, only the values inside of σ range (68%) were considered to reduce this negative effect.

$$w = [\mu - \sigma, \mu + \sigma] \qquad (2)$$

3.2 A: Initial Pose Known

In this case, an initial pose estimate (position and orientation) is completely known, and, therefore, a local based search is performed using LRF readings against the map. In order to match the data type returned from LRF readings (Cartesian points), the map line segments need to be transformed into a significant number of points to preserve data integrity as much as possible. The origin of the LRF points are translated to the given position coordinates and rotated according to the given orientation. Then, a matching procedure takes place to adjust and align the LRF points with the map points to determine the best fitting pose. To match the two point clouds and evaluate the displacement error, the Iterative Closest Point (Besl and McKay, 1992) (ICP) algorithm, represented in (3), was used.

$$R_k, t_k = \underset{R,t}{\operatorname{argmin}} \frac{1}{N} \sum_{i}^{N} \|R p_i^k + t - m_i^k\|^2 \qquad (3)$$

The map points, m, are chosen as the reference and LRF points, p, are subject to a rigid body transformations R,t that aligns the two by minimizing the quadratic error of the point to point distance metric at each k iteration for the all the N LRF points. The algorithm stops when the point association between the k and $k-1$ iterations are the same. The resultant output, R_k and t_k, is the rigid body transformation that best fits the two point clouds and is determined from SVD decomposition (K. S. Arun, 1987). By applying the result to the initial guess the final pose estimate is revealed. One major drawback in this algorithm is that the ICP can be trapped in local minima and this is the main reason why it has been chosen for local search scenario. Variations of this algorithm that matches points to lines such as (Low, 2004)and (Censi, 2008), have been proposed but the error metrics require non linear minimization metrics which are solved using approximations and are not robust against large initial displacement error. Point to point metric presents a closed form solution and converge faster despite time not being a priority in the context of this application. If the solution presents an associated error with a order of magnitude higher than the devices standard deviation (STD), the initial pose estimate was not good enough therefore other case scenarios are applied. In these other scenarios where the initial pose estimate is incomplete or non-existent, the resultant pose estimate always suffer a final ICP alignment.

3.3 B: Only Position Known

In this case only a position initial estimate is known. Taking advantage of the available information, the proposed solution consists in a brute force approach of the previous scenario. Thus the ICP algorithm is initialized for a predefined set of poses where only the estimate orientation angles vary. The chosen orientation values should be as low as possible apart so the ICP algorithm has a higher chance to converge to the optimum solution without being stuck in a local minima. The final estimated pose is given by the pose with the lowest ICP associated e_{pp}.

3.4 C: Only Orientation Known

When only the orientation initial estimate is given, again, a brute force version of ICP could be applied varying the position, but depending on the point density of the map, the successive ICP could become very computationally heavy. As an alternative, a novel method was developed consisting in using the readings as a projection of the possible location of the sensor. Every single LRF measurement is projected backwards from each map point revealing a LRF possible location. A vote is then accumulated for the respective coordinates. The coordinates which have a higher vote count determines the most likely position estimate.

3.5 D: Initial Pose Unknown

This is the worst case scenario as the LRF location can be anywhere in the map. In order to reduce the search space, when compared to the previous solutions, a different approach was taken. The method presented does not taken into account the wall installation constrain and is divided into two phases: feature extraction and matching features. A flowchart is provided on Figure 3, which depicts the following different phases and main steps involved in this case scenario.

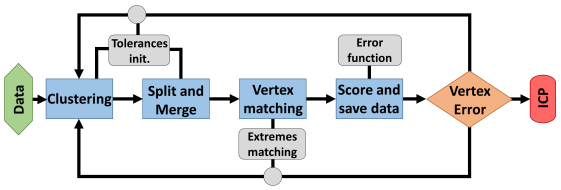

Figure 3: Flowchart of scenario D.

3.5.1 Feature Extraction

The objective in this phase is to extract line segments and vertex points from the processed LRF output data. A comparison between some of the most common line extraction methods is present in (Viet Nguyen, 2007). Based on the conclusions, the most correct and best suited method for the localization problem with an a priori map was the Split and Merge technique preceded by a clustering algorithm. So the first step is to perform a primary classification of points using a clustering technique. The Distance based Convolution Clustering (DCC) proposed by (Carlos Fernández, 2010) was used. It consists on identifying break points based on a sudden change of the distance between consecutive scan points, and once one is found a new cluster is created. To do that, a high pass filter is applied to the set of euclidean distances between consecutive points. The break points are identified where the convolution is greater than a cluster threshold whose value is proportional to the LRF readings standard deviation. Wrong or missing breakpoint identification can happen as this is a simple and primary approach. The following step uses the Split and Merge algorithm to confirm and correct for those erroneous cases in order to finally extract lines and vertex points. The Split and Merge technique begins by the splinting phase where the objective is to create sub-clusters of a cluster based on the evidence of a line pattern points. A line fits the points using an ordinary least squares line fitting technique and a breakpoint is identified if the most distant point to the line is greater than a given split threshold. Since the previous procedures can wrongly create more than one line segment for the same correspondent line in the map, a merging phase is conducted to unify similar clusters. If two neighbor segments have its respective, angle difference inferior to a given slope threshold, and distance between two extreme points inferior to a proximity threshold, the two respective clusters are unified. The segment line parameters, for this unified cluster, are extracted, this time, using a M estimator robust line regression technique with a bi-square weight function. Vertex points are extracted extending and intercepting consecutive and close enough line segment extremes.

3.5.2 Feature Matching

The matching phase takes advantage of the geometric features extracted previously, specially the vertexes. An extraction of map vertexes is first performed, and then, a matching hypotheses is formed for every pair combinations of map vertexes and extracted vertexes. Assuming a vertex is the common extreme point of two different line segments, after overlapping the two vertex points in the pair by a translation transformation means, there exists a four possible pair combinations of alignments for the vertexes respective line segments. This alignments are done by means of rota-

tions. The extracted rigid body transformation is applied to all LRF points and after this transformation the pp error function in (1) is used to assess and evaluate the displacement between the two point clouds. The resultant estimated pose, $\hat{P}_f$, is determined from the transformation that yields the lowest error. In case no vertexes are extracted, threshold values that affect the feature extraction phase are changed and the procedure is repeated. If the combinations of tested threshold values are not enough to produce a valid result, i.e., a result whose the point to point error value is relatively close to the devices standard deviation, an extremes matching method is applied. This method procedure is similar to the vertex method except it uses end points of extracted line segments instead of vertexes. For every pair of points (one map vertex and one end point from an extracted line) a two combination matching (instead of four) is done by aligning the line segment with the two map lines that originate the map vertex in question.

4 SIMULATED RESULTS

4.1 LRF Simulation

To test and confirm the proposed solution, a simulator was developed which is composed by two parts: the LRF model and LRF scan procedure. The two are intimately linked as the model contains the device properties that influence the scan result. Noise source, in LRF devices, mostly comes from internal electronics generating jitter, walk nonlinearity, and drift (Markus-Christian Amann, 2000) which affect sensor accuracy not only by distance reading means but angular steps also suffer from deviation despite being almost insignificant. To simulate noise, a normal distribution, with zero mean and standard deviation given by manufacturer, was chosen to model the deviation from the correct value, p_i. This point is obtained in the simulator by intercepting every sensor ray with every wall and selecting the appropriate point. The coordinates of a point affected by noise, p_n, is given by (4).

$$p_n = T_v(\zeta_l) * (p_a(\zeta_a, \vec{r}_i)) \quad (4)$$

It should be noted that linear and angular noise are not commutative operations due to the nonlinearity of map. That being said, first, the p_a is obtained from provoking an angular deviation ζ_a to $\vec{r}_i$ yielding $\vec{r}_n$. Then $T_v(\zeta_l)$ applies a linear deviation of ζ_l in the direction of $\vec{r}_n$ (see Figure 2). A value for the LRF range parameter is often given by the manufacturers under certain ideal conditions and a range correction factor is often provided to compensate for changes of these conditions. For simulation purpose meteorologic conditions are assumed fine with no influence on readings. The target reflectivity coefficient indicates the amount of energy it is capable to reflect. As far away a target is, the higher the reflectivity necessary to a LRF detect the reflected beam. This dependence characteristic, often present in LRF manuals, was implemented in the simulator to validate the readings. Walls shape were considered diffuse so the target reflectivity value seen by the LRF is corrected by a cosine of the incidence angle factor. Due to the lack of information inherent of a two dimensional map representation, neither color or target size influences were taken into account in the simulation scan process. As for resolution limits, linear resolution was implemented rounding the distance value, $\|r_n\|$, to the level of uncertainty of the LRF model, and angular resolution is the value that determines the angle α_i of each ray scan line given the configurable field of view (FOV) value. The output is composed by a set of $\|r_n\|$ distance measurements and the associated α_i angles. Reflectivity can also be returned for some models.

4.2 Results

To evaluate the algorithm performance, tests were performed in simulation environment. Due to the nature of simulation, the true pose is available to compare against the results. Four tests were performed for each map, each of the tests for different scenarios as described in Section 3. Two maps, converted to points with a density of 50 points per meter, with no outliers in both, were used. The first one is a simple created asymmetrical map and the other a complex map from ITER basement, where the actual CPRHS will navigate, represented respectively from left to right in Figure 4.

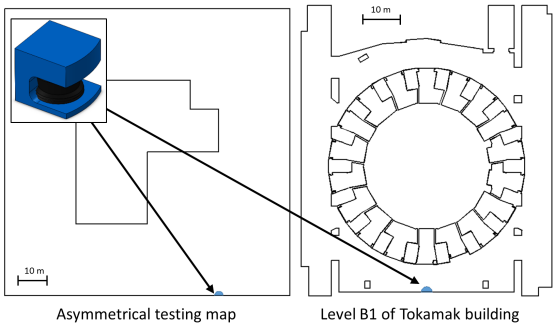

Figure 4: LRF sensor used in simulation testing scenarios.

For each a model of a LRF was created featuring the following main properties: 180° of FOV, STD of ±50 mm, maximum range of 100 m, linear resolution of 1 mm and angular resolution of 0.5°. Each LRF

were set in the predefined poses represented in Figure 4, from where only one scan was taken. In scenario D, the tolerance values that gave the best results, for the clustering and feature extraction were the following: 0.5 m for proximity, 5° for slope, 1 m for clustering and 0.5 m for split.

The results obtained for the simple asymmetrical map and for ITER map are presented in table 1. $\hat{P}_t$ indicates the exact true pose where the measures were taken from, $\hat{P}_i$ is an initial guess, at least, 1 meter away from the true position, $\hat{P}_f$ is the final pose resulting from the algorithm output, "pp err." is the point to point error given by (1), "abs. error" is the difference between true pose and final pose and "RT" (run time) is the time elapsed in the algorithm execution[1]. Images of the results are displayed respectively in Figures 5 and 6. In each figure three images are displayed: at the left side the ICP resultant alignment of LRF points (in red) and the respective iterative evolution from $\hat{P}_i$ to $\hat{P}_f$, the heat map resulting from the voting method is shown on the upper right section, and on the lower section the geometrical features extracted (vertexes represented by the small circles) in the vertex method are pictured. For scenario B an array of 13 different and equally spaced angle values were used and the result is not displayed because it is similar to the ICP result.

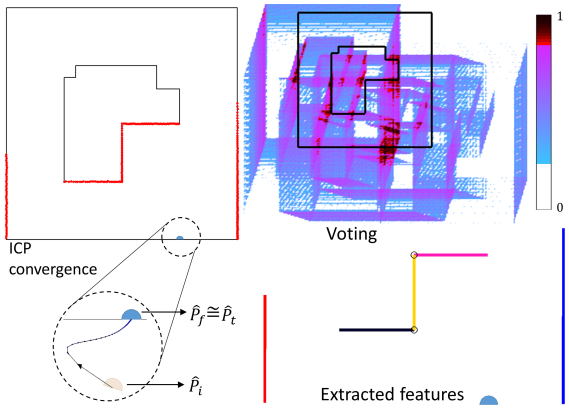

Figure 5: Simulation results for asymmetrical map.

5 FIELD RESULTS

5.1 Sensors Specification

The LRF device used was a Hokuyo URG-04LX-UG01 (see Figure 7). The following main specifications were taken from the respective device manual:

[1]tests were always done on the same machine, an i5 processor.

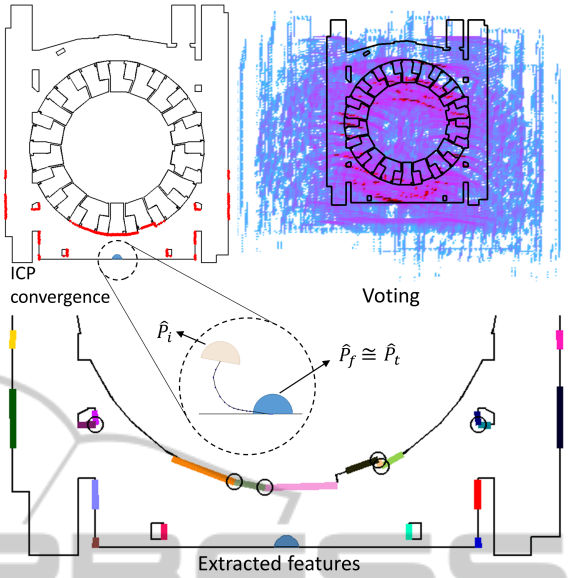

Figure 6: Simulation results for ITER map.

240° of FOV, STD of ±50 mm, maximum range of 4 m, linear resolution of 1 mm and angular resolution of 0.36°. The LRF sensor was set in a predefined measured position and orientation shown in Figure 7. At least, data from one hundred scans were gathered and processed to reject discrepant value measurements. In scenario D, the tolerance values that gave the best results, for the clustering and feature extraction were the following: 0.1 m for proximity, 15° for slope, 0.1 m for clustering and 50 mm for split.

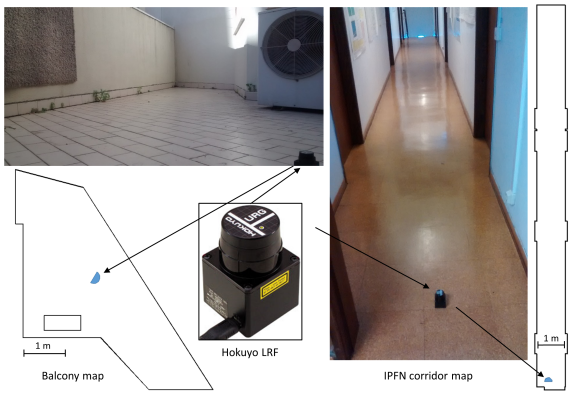

Figure 7: LRF sensor, photos and maps used in experimental testing.

5.2 Field Tests

Two distinct maps were used in the field test as well, one from a house balcony which contain some outliers, and the other from an office corridor (Figure 7) composing a common environment of doors and long walls. Both maps were converted to points with

Table 1: Experimental results table.

	Map	Scen.	$\hat{P}_t$ [m, m, °]	$\hat{P}_i$ [m, m, °]	$\hat{P}_f$ [m, m, °]	pp err. [mm]	Abs. err. [mm, °]	RT[s]
Simulated Scenarios	Asymm.	A	(75.000, 0.000, 90.0)	(73.550,-5.280,73.0)	(75.004, 0.002, 90.0)	53.1	(4.1, 0.0)	4.2
		B		(73.550, -5.280, -)	(75.008, 0.007, 90.0)	53.1	(10.4, 0.0)	59
		C		(-, -, 73.0)	(65.752, 0.852, 73.0)	4050.3	(9286.9, 17.0)	212
		D		(-, -, -)	(75.013, 0.011, 90.0)	53.4	(17.4, 0.0)	5
	ITER	A	(33.750, 1.000, 90.0)	(32.750, 2.000, 80.0)	(33.750, 1.002, 89.9)	50.6	(2.0, 0.1)	4.3
		B		(32.750, 2.000, -)	(33.750, 1.002, 89.9)	50.6	(2.0, 0.1)	48
		C		(-, -, 80.0)	(27.303, 1.716, 80.0)	1928.5	(6487.0, 10.0)	1143
		D		(-, -, -)	(33.713, 0.989, 90.0)	82.8	(38.5, 0.0)	33
	Map	Scen.	$\hat{P}_m$ [m, m, °]	$\hat{P}_i$ [m, m, °]	$\hat{P}_f$ [m, m, °]	pp err. [mm]	Rel. err. [mm, °]	RT[s]
Real Scenarios	Balcony	A	(1.700, 1.400, 330.0)	(1.700, 1.400, 330.0)	(1.699, 1.452, 329.2)	44.6	(52.5, 0.8)	0.38
		B		(1.700, 1.400, -)	(1.699, 1.452, 329.2)	44.6	(52.5, 0.8)	4.3
		C		(-, -, 330.0)	(1.667, 1.457, 330.0)	79.6	(66.1, 0.0)	135
		D		(-, -, -)	(1.599, 1.490, 330.7)	70.8	(64.3, 0.7)	1.4
	IPFN	A	(14.750, 0.700, 180.0)	(14.750, 0.700, 180.0)	(14.713, 0.665, 178.7)	26.3	(51.0, 1.3)	0.44
		B		(14.750, 0.700, -)	(14.713, 0.665, 178.7)	26.3	(53.0, 1.3)	6.4
		C		(-, -, 180.0)	(14.728, 0.707, 180.0)	41.6	(23.0, 0.0)	279
		D		(-, -, -)	(14.720, 0.665, 178.7)	26.4	(46.7, 1.3)	7

a density of 50 points per meter except for the voting tests where the density was changed to 5 in order to terminate the algorithm execution in a feasible time. The results obtained for the balcony and corridor maps are presented in table 1. The respective section columns are identical to the columns of the simulated results explained before except for $\hat{P}_m$ which means pose measurements, consisting the only way to first guess the initial pose (by hand measuring) so a relative error column ("Rel. err") was introduced. Also images of the respective results are displayed in Figures 8 and 9. The images follow the same layout as the simulation figures stated above.

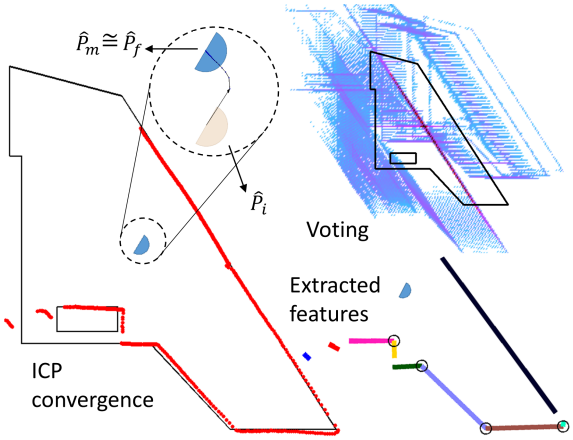

Figure 8: Balcony map experimental results.

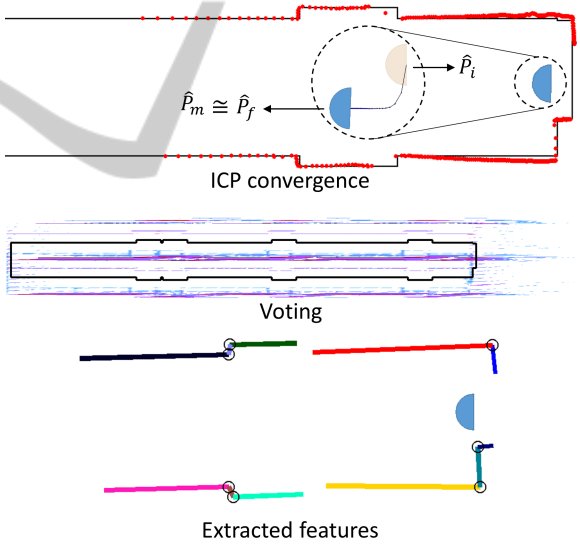

Figure 9: IPFN map experimental results.

6 CONCLUSIONS

An algorithm to calibrate a LRF sensor network was proposed. The outcome is an estimated pose for each device in the network. Simulated and experimental test results show a dependency of the pose estimate error to the sensor and map description accuracy. The developed algorithm receives three input parameters: a map description of the environment, LRF data, and an initial pose estimate for each device. The first two are mandatory and the uncertainty associated with the

last one defines a scenario which determines the algorithm behavior. Regardless of the scenario, the map is always converted to points in order to assess the results using (1). The map point conversion density should be chosen accordingly as the previous equation presents an $O(n^2)$ operation.

Whenever an initial pose estimate is completely known, the ICP algorithm is executed. The final pose estimate is revealed by applying the ICP resultant rigid body transformation to the initial pose estimate. This is the fastest and most accurate method but isn't robust against the presence of outliers in the LRF data or map description. To reduce this negative effect, an outlier rejection method is planned for future work.

An extreme scenario may occur when the pose of the sensors is completely unknown. In this case, ICP alone cannot be used because of its local minima problem, therefore a developed vertex method is applied. This method comprises two phases: first, geometric features, as segment lines and vertexes, are extracted and subsequently a matching technique based on the geometric combination of these features is preformed. The main obstacle here is to figure out the best combination of threshold values that leads to a correct feature extraction. The time complexity is proportional to the number of extracted features. Other techniques, not as reliant on threshold values, are on future plans. As an alternative, a brute force test was conducted where the map was divided in a grid and for each point of the grid, the ICP was executed. The results for the asymmetrical map are shown in Figure 10. Although much more time consuming than the vertex method, slightly better accurate results were achieved.

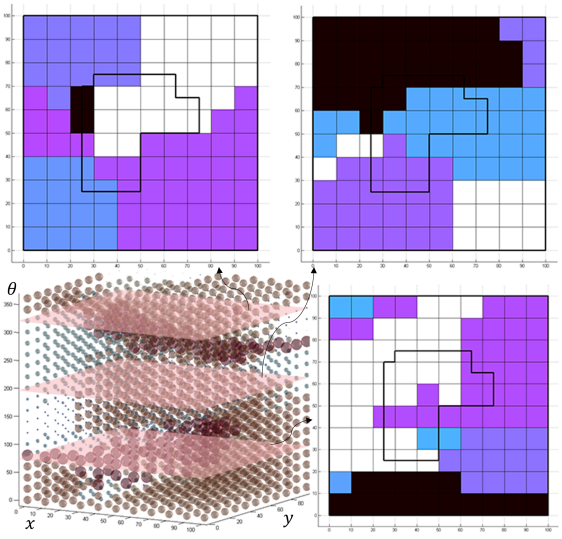

Figure 10: ICP brute force result.

As for the intermediate scenario, only the position or orientation estimate value is known. In the first case, a brute force ICP is carried out in the given position for a set of predefined angles. For the second case, a voting based algorithm is applied to assign a estimate probability of the LRF position to each of the map coordinates. The voting method can be time consuming and a less accurate method due to a combinations of high initial angle deviation, low map resolution and symmetry. Nevertheless suggests a consistent alternative and a case of study for a global search method.

An accurate map is assumed although, in a real case scenario, that might not be the case. In the presence of outliers in the scanned data or map misdescription, robustness tests show that a variation of 1% is enough to produce an error ten times higher. These results, in the case of this application, can compromise the localization algorithm behavior, where the poses of the devices are to be used. In order to improve outliers robustness, the ICP algorithm can be customized to include an outliers rejection method.

ACKNOWLEDGEMENTS

The work leading to this publication received financial support from "Fundação para a Ciência e Tecnologia" through project UID/FIS/50010/2013. This publication reflects the views only of the author, and Fusion for Energy cannot be held responsible for any use which may be made of the information contained therein.

REFERENCES

A. Tesini, J. P. (2008). The iter remote maintenance system. *Fusion Eng. Des.*, 83(7-9):810–816.

Antone, M. and Friedman, Y. (2007). Fully automated laser range calibration. In *Proc. BMVC*, pages 66.1–66.10. doi:10.5244/C.21.66.

Besl, P. and McKay, N. (1992). A method for registration two 3-d shapes. *IEEE Trans. Pattern Anal. and Mach. Intell.*, 14(2):239–256.

Carlos Fernández, Vidal Moreno, B. C. (2010). Clustering and line detection in laser range measurements. *Robotics and Autonomous Sys.*, 58(5):720–726.

Censi, A. (2008). An ICP variant using a point-to-line metric. *Robotics and Automation*, pages 19–25.

Darren Locke, C. G. (2014). Progress in the conceptual design of the iter cask and plug remote handling system. *Fusion Eng. Des.*, 89(9-10):2419–2424.

J. Ferreira, A. Vale, R. V. (2013). Vehicle localization system using off-board range sensor network. *Proc. of*

the 8th IFAC Intelligent Autonomous Vehicles Symposium, 8(1):102–107.

J. Soares, R. Ventura, A. V. (2014). Human-robot interface architecture for a multi-purpose rescue vehicle for remote assistance. In *Symposium on Fusion Technology*.

K. S. Arun, T. S. Huang, S. D. B. (1987). Least-squares fitting of two 3-d point sets. *Pattern Analysis and Machine Intelligence, IEEE Transactions*, 9(5):698–700.

K. Schenk, A. K. (2012). Automatic calibration of a stationary network of laser range finders by matching movement trajectories. *IEEE/RSJ Int. Conf. on Intelligent Robots and Systems*, pages 431–437.

Low, K.-L. (2004). Linear least-squares optimization for point-to-plane ICP surface registration. Tech. report.

Markus-Christian Amann, Thierry Bosch, M. L. R. M. M. R. (2000). Laser ranging: a critical review of usual techniques for distance measurement. *Opt. Eng.*, 40(1):10–19.

Sebastian Thrun, J. L. (2008). *Handbook of Robotics*. Springer.

Viet Nguyen, Stefan Gächter, A. M. N. T. R. S. (2007). A comparison of line extraction algorithms using 2d range data for indoor mobile robotics. *Autonomous Robots*, 23(2):97–111.

Vincenzo Caglioti, Alessandro Giusti, D. M. (2008). Mutual calibration of a camera and a laser rangefinder. *Proc. Int'l Conf. on Computer Vision Theory and Applications*, pages 33–42.